

Electronic Supplementary Information for:

Photoswitching chiroptical response in camphorate-based chiral metal-organic frameworks

Katelyn M. Clutterbuck,^a Hunter J. Windsor,^a Deanna M. D'Alessandro^{*b} and Girish Lakhwani^{*a}

^a School of Chemistry, The University of Sydney, Camperdown, New South Wales 2006, Australia.

^b School of Chemical and Biomolecular Engineering, Faculty of Engineering, The University of Sydney, Darlington, New South Wales 2006, Australia.

*Email: deanna.dalessandro@sydney.edu.au, girish.lakhwani@sydney.edu.au

Table of Contents

Experimental	2
Structure of Ligands	5
Crystallographic Data.....	6
Powder Diffraction Data	8
Thermogravimetric Analysis Data	9
Electron Paramagnetic Resonance (EPR) Spectra	10
EPR Decay Curves	11
UV-Visible spectra	12
Near-IR spectra	13
Circular Dichroism (CD) Spectra.....	14
Supporting Crystal Structure Images of D-Cd-MOF	16
CD Reversibility Studies in Cd-MOF	17
References	18

Experimental

General Procedures

All reagents and solvents other than those stated below were obtained from commercial sources and used without further purification. Samples were irradiated using a Weltool M2-BF Purple Beard UV flashlight that emits at a wavelength of 365 nm.

Single crystal X-ray data collections were performed using a Rigaku XtaLAB Synergy-DW Custom diffractometer equipped with an FR-X rotating-anode source outputting confocal mirror-monochromated Cu-K α radiation ($\lambda = 1.54184 \text{ \AA}$) and a Rigaku HyPix-6000HE detector. Data were collected about ω scans and then were integrated and reduced with absorption corrections (Gaussian grid face-indexed numerical integration with beam profile) being applied using CrysAlisPro. Structure solutions were obtained by intrinsic phasing using SHELXT¹ and were refined by full-matrix least-squares on all unique F^2 values using SHELXL² as implemented within the OLEX2-1.5 GUI.³ Molecular structure drawings were made using CrystalMaker 11 version 11.0.2. The full details used in each structure refinement model for **D-Zn-MOF** (CCDC: 2432916) and **D-Cd-MOF** (CCDC: 2432917) can be found in their respective crystallographic information files. Powder X-ray diffraction (PXRD) measurements were collected on a PANalytical X'Pert Pro MPD instrument diffractometer operating in Debye-Scherrer geometry with Cu K α X-ray radiation ($K\alpha_1 = 1.540598 \text{ \AA}$, $K\alpha_2 = 1.544426 \text{ \AA}$) and a PIXcel1D detector in continuous scanning mode. Samples were contained in flame-sealed thin-walled glass capillaries with an internal diameter of 0.5 mm that were rotated at room temperature during the measurements. Thermogravimetric analysis (TGA) measurements were obtained on a TA Instruments Discovery TGA under an air flow of 20 mL/min at a ramp rate of 10° C/min from 25°C to 600° C in an aluminium pan. Solid state diffuse reflectance UV/Vis spectroscopy were taken using an Agilent Cary5000 UV/Vis/Near-IR spectrophotometer equipped with a Harrick Praying Mantis accessory in the region of 50000-12500 cm⁻¹. Solution state UV/Visible spectroscopic measurements were taken on a Cary60 spectrophotometer with samples held in a 1 cm quartz cuvette. Near-IR spectroscopic measurements were taken using a Bruker MPA spectrometer. Spectra were collected over the region of 10000-4000 cm⁻¹ with 64 scans at a spectral resolution of 8 cm⁻¹. Samples were measured in a suspension of EtOH. Electron Paramagnetic Resonance (EPR) spectroscopy data was collected at room temperature on a Bruker benchtop EMX EPR spectrometer interfaced with Xenon_nano software. Field Sweep measurements were made at a modulator amplitude of 1.0 G with a received gain tuned to prevent signal saturation and were referenced to a strong pitch. Time Sweep measurements were performed at a resolution of 5243 seconds and a time constant of 1311 seconds. Raw EPR decay curves fitted to an exponential decay using OriginPro 2022 software. Nuclear Magnetic Resonance (NMR) spectroscopic measurements were taken on a Bruker AVIII 400 MHz NMR Spectrometer. Mass spectrometry measurements were taken on Bruker amaZon SL ESI mass spectrometer. Circular dichroism (CD) measurements were taken using a JASCO-1500 spectrophotometer. Samples were dispersed in EtOH by sonication before collecting measurement in a 1 cm quartz cuvette. Absorbance measurements were corrected according to Equation 1.¹ A_{corr} is the corrected absorbance, A_{raw} is the uncorrected absorbance, and M and R are constants representing the Mie and Rayleigh contributions respectively.

$$A_{corr} = A_{raw} - \left(M - \frac{R}{\lambda^4} \right)$$

Equation 1

Synthesis of N'N'-di(4-pyridyl)-naphthalene tetracarboxylic diimide (DPNDI)

N'N'-di(4-pyridyl)-naphthalene tetracarboxylic diimide (DPNDI) was synthesised through a modified literature procedure.⁵ Naphthalene tetracarboxylic anhydride (3.07 g, 11.5 mmol) and 4-aminopyridine (2.39 g, 25 mmol) were refluxed in dry DMF (45 mL) for 18 hrs under an N₂ atmosphere. The mixture

was allowed to cool to room temperature before being poured over ice (approx. 100 mL). Once melted, the precipitate was collected via vacuum filtration, washing with acetone and further dried overnight under vacuum to yield a fine beige powder (4.618 g, 10.9 mmol, 96% yield). $^1\text{H NMR}$ (400 MHz, CF_3COOD): δ = 9.19 (d, J = 7.1 Hz, 4H), 9.12 (s, 4H), 8.45 (d, J = 7.1 Hz, 4H) ppm. $^{13}\text{C NMR}$ (400 MHz, CF_3COOD): δ = 165.19, 155.20, 145.49, 135.35, 131.76, 130.04, 129.14 ppm. **ESI-MS**: m/z : $[\text{MH}]^+$ calculated for $\text{C}_{20}\text{H}_{10}\text{N}_4\text{O}_4$: 421.09; found 421.09, $[\text{M}+\text{Na}]^+$ calculated for $\text{C}_{20}\text{H}_9\text{N}_4\text{O}_4\text{Na}$: 443.08; found 443.05.

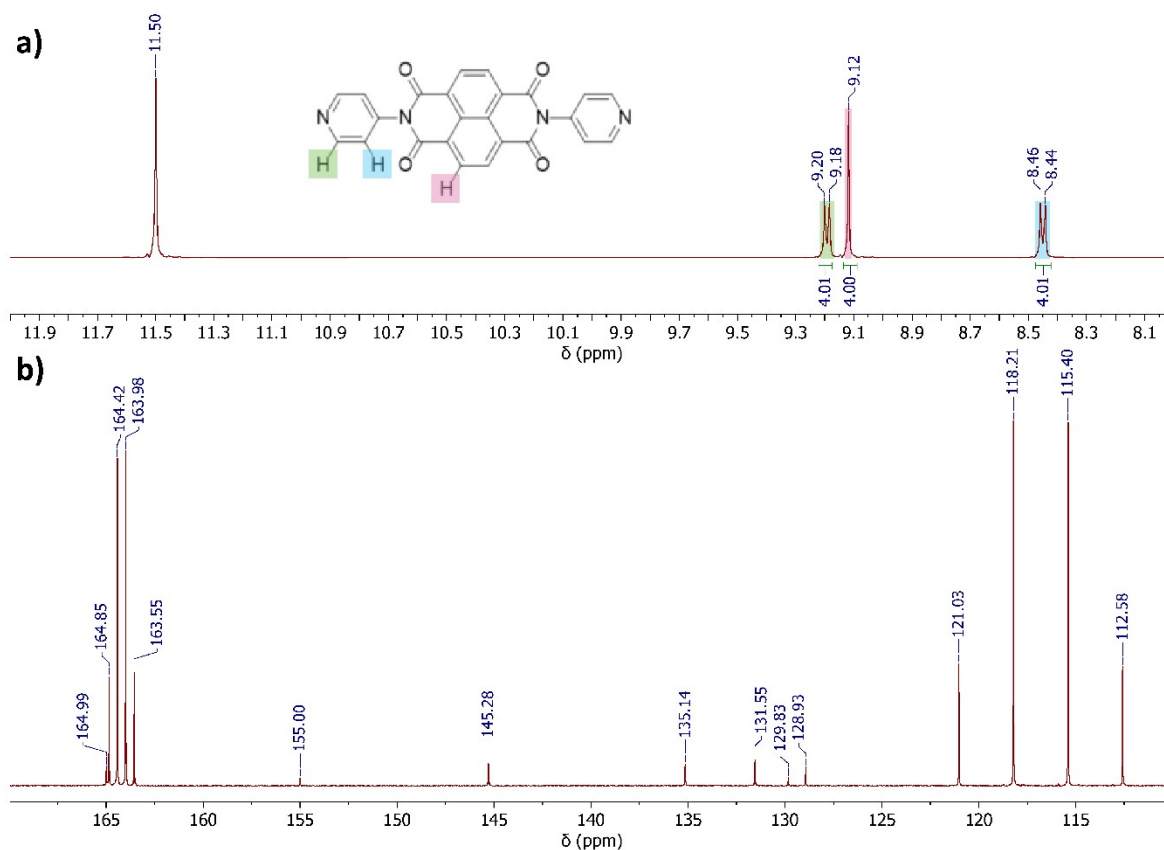


Figure S1: a) $^1\text{H NMR}$ spectrum of DPNDI (400 MHz, CF_3COOD). Peak at 11.5 ppm is due to solvent; b) $^{13}\text{C NMR}$ spectrum of DPNDI (400 MHz, CF_3COOD). Quartet peaks at 164.2 and 116.8 ppm are due to solvent.

Synthesis of $[\text{Zn}_4(\text{D-cam})_4(\text{DPNDI})_2]\cdot 3\text{DMF}$ (**D-Zn-MOF**)

Single crystals for SCXRD: $\text{Zn}(\text{NO}_3)_2\cdot 6\text{H}_2\text{O}$ (7.4 mg, 0.025 mmol) and NaOH (2 mg, 0.05 mmol) were placed in a 2 mL cylindrical vial and placed within a 21 mL scintillation vial containing D-cam (5 mg, 0.025 mmol) and DPNDI (10.5 mg, 0.025 mmol). The 2 mL vial was filled to the brim with EtOH and the 21 mL vial was filled to the top of the inner vial with DMF. The vial was sealed and solutions allowed to diffuse for six weeks to yield single crystals of **D-Zn-MOF** for SCXRD analysis.

Bulk product: $\text{Zn}(\text{NO}_3)_2\cdot 6\text{H}_2\text{O}$ (7.4 mg, 0.025 mmol) was dissolved in EtOH (1 mL) and added to a solution of containing D-cam (5 mg, 0.025 mmol) and DPNDI (10.5 mg, 0.025 mmol) in DMF (5 mL) at 80° C. After 48 hours, the orange square plate shaped crystals that were washed in DMF and EtOH before being dried under a stream of N_2 to yield **D-Zn-MOF** (7 mg).

Synthesis of $[\text{Zn}_4(\text{L-cam})_4(\text{DPNDI})_2]\cdot 3\text{DMF}$ (L-Zn-MOF)

L-Zn-MOF was synthesised in bulk in the same conditions as **D-Zn-MOF**, only using L-cam instead of D-cam to yield **L-Zn-MOF** (7 mg).

Synthesis of $[\text{Cd}_4(\text{D-cam})_4(\text{DPNDI})_4]\cdot 3\text{EtOH}\cdot 5\text{DMF}$ (D-Cd-MOF)

Single crystals for SCXRD: DPNDI (10.5 mg, 0.025 mmol) and D-cam (5 mg, 0.025 mmol) were dissolved in 5 mL DMF and heated to 80° C in a 21 mL scintillation vial. A solution of $\text{Cd}(\text{NO}_3)_2\cdot 4\text{H}_2\text{O}$ (7.7 mg, 0.25 mmol) in 5 mL EtOH was added to the vial and allowed to sit at 80° C for a further 48 hours to yield single crystals of **D-Cd-MOF** for SCXRD analysis.

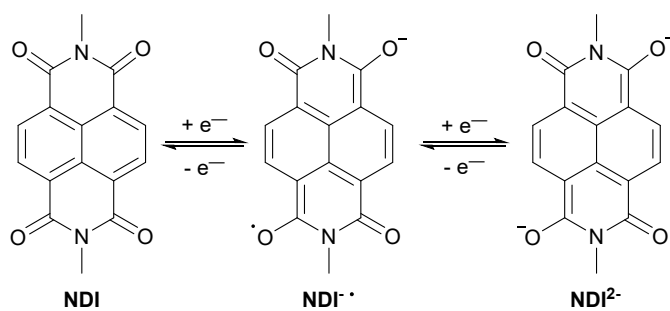
Bulk product: DPNDI (10.5 mg, 0.025 mmol) and D-cam (5 mg, 0.025 mmol) were dissolved in DMF (10 mL) and heated to 80° C in a 21 mL scintillation vial. A solution of $\text{Cd}(\text{NO}_3)_2\cdot 4\text{H}_2\text{O}$ (7.7 mg, 0.25 mmol) in 10 mL EtOH was added to the vial, followed by 25 μL of a 0.1 M Li(OAc) in MeOH solution and allowed to sit at 80° C for a further 48 hours to yield **D-Cd-MOF** (15 mg).

Synthesis of $[\text{Cd}_4(\text{L-cam})_4(\text{DPNDI})_4]\cdot 3\text{EtOH}\cdot 5\text{DMF}$ (L-Cd-MOF)

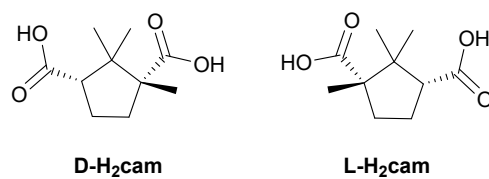
L-Cd-MOF was synthesised in bulk in the same conditions as **D-Cd-MOF**, only using L-cam instead of D-cam, to yield **L-Cd-MOF** (15 mg).

Structure of Ligands

a)



b)



Scheme S1: a) Structure and redox states of the NDI core and b) structures of the enantiomeric pair D-H₂cam and L-H₂cam.

Crystallographic Data

Table S1: Crystallographic Data for **D-Zn-MOF** and **D-Cd-MOF**.

Compound	D-Zn-MOF	D-Cd-MOF
Empirical formula	C _{31.98} H _{43.28} N _{5.33} O _{9.33} Zn	C ₁₅₇ H ₁₅₇ Cd ₄ N ₂₁ O ₄₀
Formula weight	717.03	3427.63
Temperature /K	150.00(10)	150.00(10)
Crystal system	orthorhombic	triclinic
Space group	<i>P</i> 2 ₁ 2 ₁ 2	<i>P</i> 1
a/Å	13.2755(5)	13.6882(3)
b/Å	13.2994(5)	18.2052(3)
c/Å	22.3069(10)	20.0158(2)
α/°	90	63.0610(10)
β/°	90	82.3530(10)
γ/°	90	89.181(2)
Volume/Å³	3938.4(3)	4401.11(13)
Z	4	1
ρ_{calc}/cm³	1.209	1.293
μ/mm⁻¹	1.315	4.454
F(000)	1508	1758.0
Crystal size/mm³	0.14 × 0.07 × 0.03	0.19 × 0.12 × 0.09
Radiation	Cu Kα (λ = 1.54184)	Cu Kα (λ = 1.54184)
2θ range for data collection/°	7.74 to 100.85	5.004 to 146.976
Index ranges	-13 ≤ h ≤ 12, -13 ≤ k ≤ 13, -22 ≤ l ≤ 22	-16 ≤ h ≤ 17, -19 ≤ k ≤ 22, -24 ≤ l ≤ 24
Reflections collected	16666	302312
Independent reflections	4042 [R _{int} =0.0749, R _{sigma} = 0.0526]	31426 [R _{int} = 0.1266, R _{sigma} = 0.0455]
Data/restraints/parameters	4042/269/288	31426/2184/1639
Goodness-of-fit on F²	1.388	1.278
Final R indexes [I ≥ 2σ (I)]	R ₁ = 0.1165, wR ₂ = 0.3260	R ₁ = 0.0991, wR ₂ = 0.2952
Final R indexes [all data]	R ₁ = 0.1523, wR ₂ = 0.3634	R ₁ = 0.1102, wR ₂ = 0.3088
Largest diff. peak/hole / e Å⁻³	1.17/-0.88	1.73/-2.13
Flack parameter	0.19(18)	0.278(12)

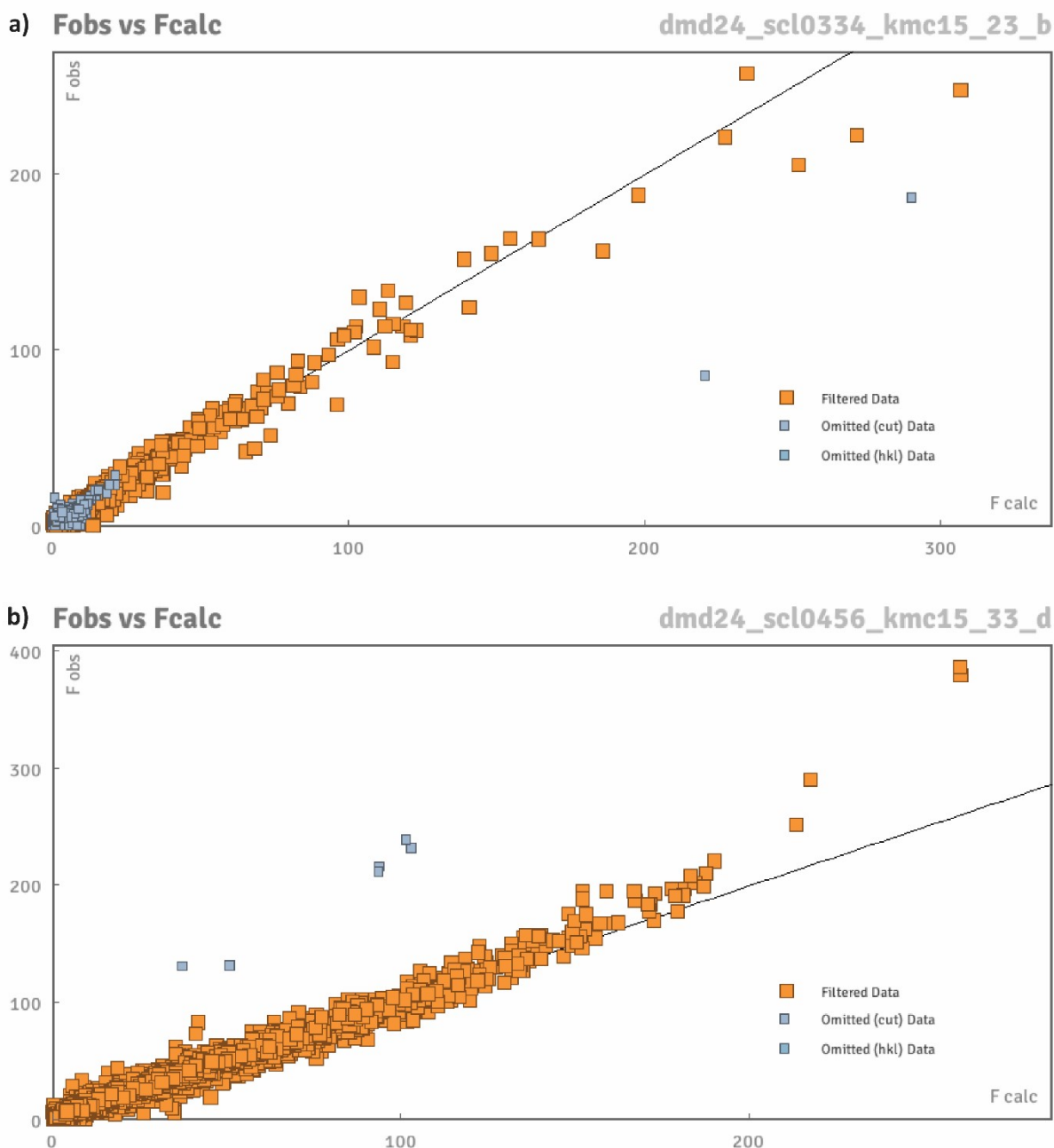


Figure S2: a) F_o vs F_c plot for **D-Zn-MOF**. Many of the low and high angle F_o values are underestimated, which may indicate the presence of extinction. However, although refining the extinction parameter results in a minor improvement in the model, the refined EXTI parameter is non-sensical given its error being too large and as such was not included in the final refinement; b) F_o vs F_c plot for **D-Cd-MOF**. Many of the F_o values are overestimated (more apparent at high angle) which may indicate the presence of unresolved twinning. However, at this stage, we cannot rule out other errors that may be associated with the data on account of the weakly diffracting data crystal.

Powder Diffraction Data

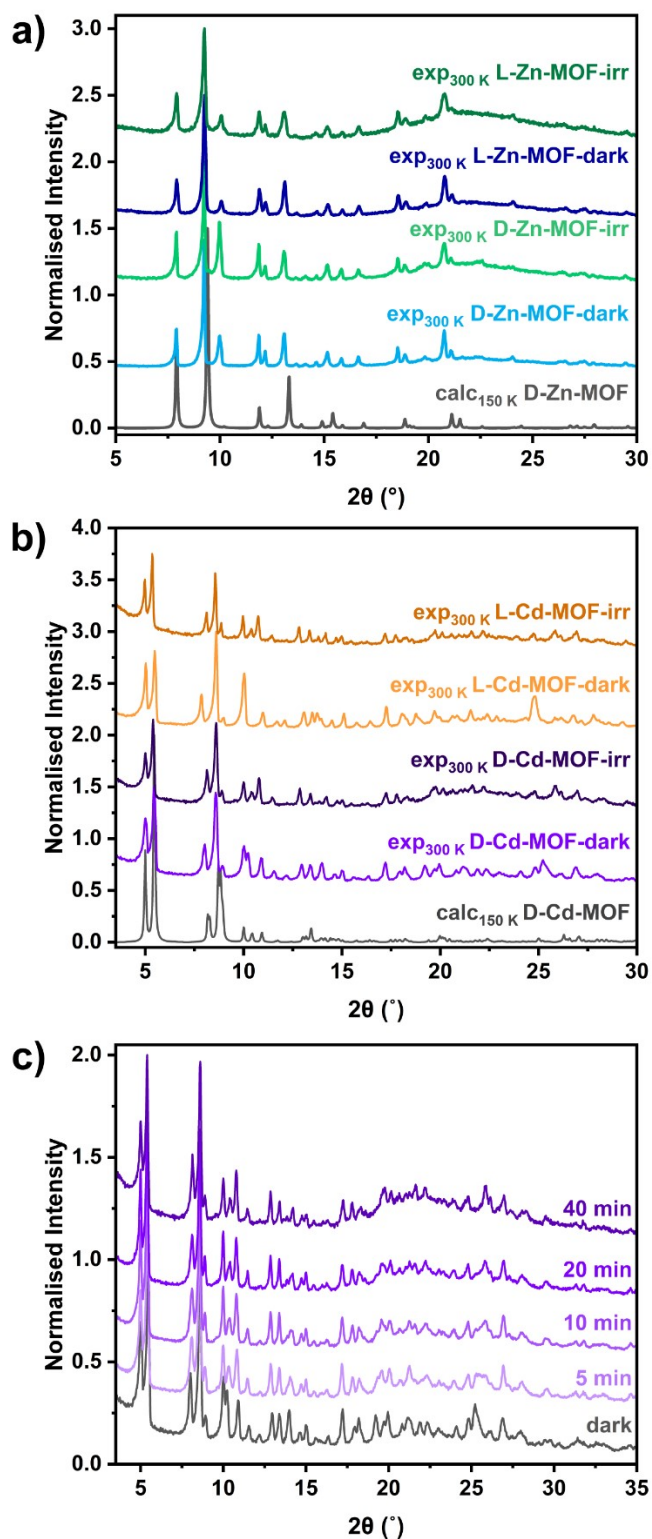


Figure S3: PXRD patterns of a) dark and irradiated (irr) D- and L-Zn-MOF bulk samples, b) dark and irradiated (irr) D- and L-Cd-MOF bulk samples, and c) D-Cd-MOF at increasing irradiation times.

Thermogravimetric Analysis Data

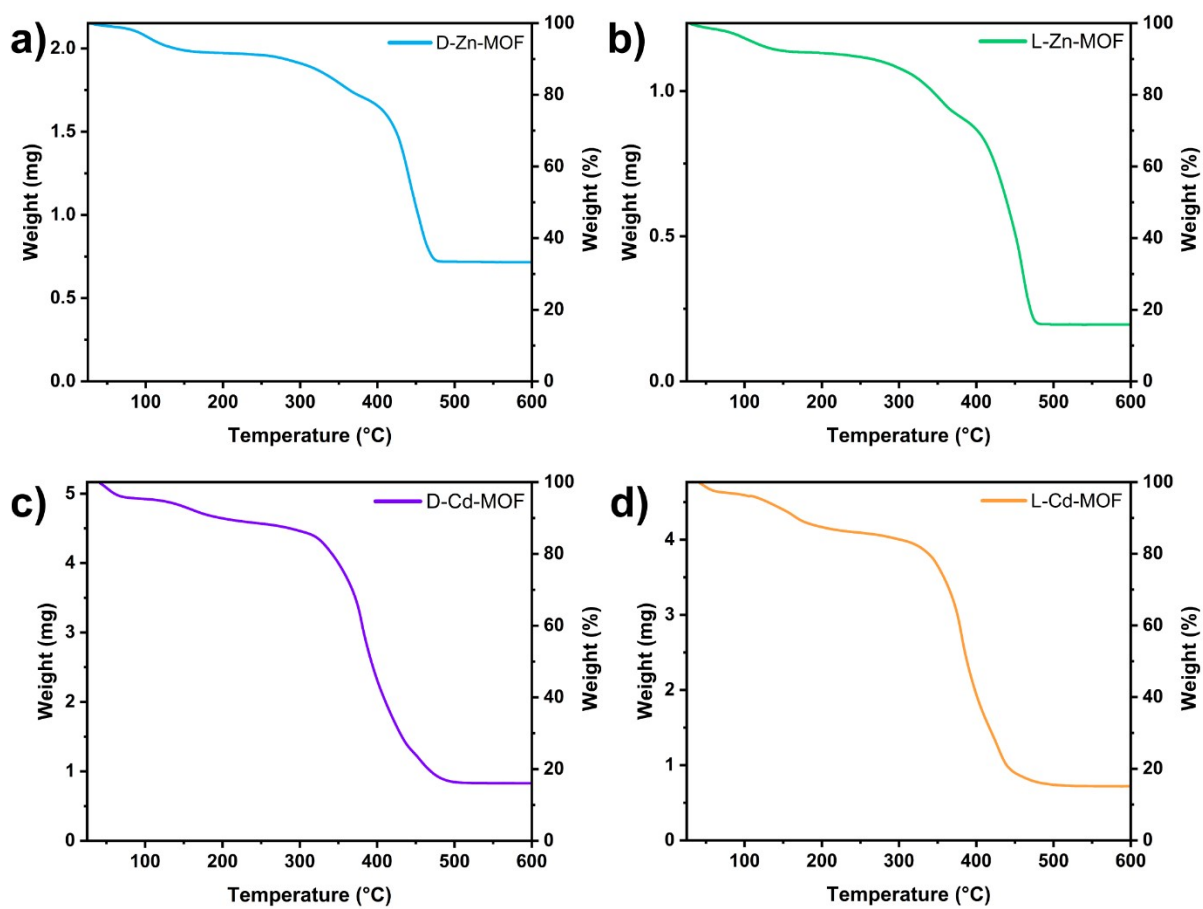


Figure S4: Thermogravimetric decay curves of a) **D-Zn-MOF**, b) **L-Zn-MOF**, c) **D-Cd-MOF** and d) **L-Cd-MOF**.

Electron Paramagnetic Resonance (EPR) Spectra

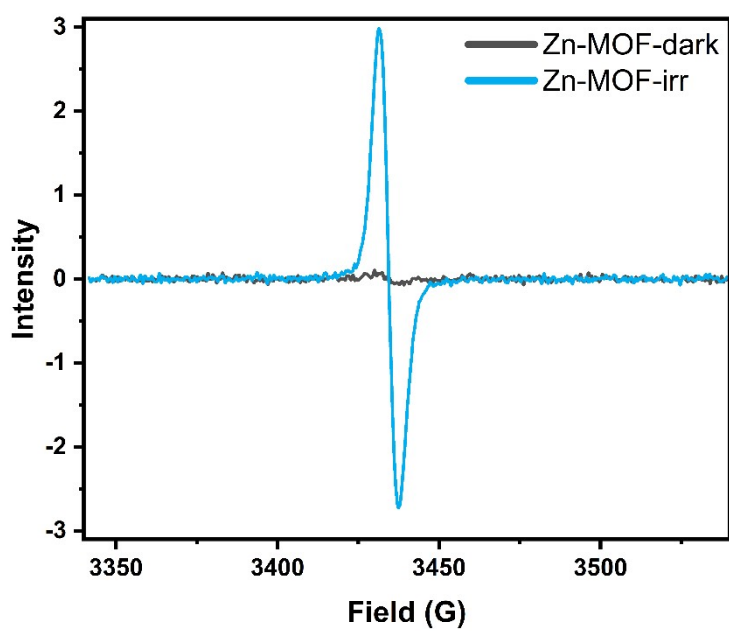


Figure S5: Overlaid EPR spectra of **Zn-MOF** before (dark) and after irradiation (irr) with 365 nm light for one minute.

EPR Decay Curves

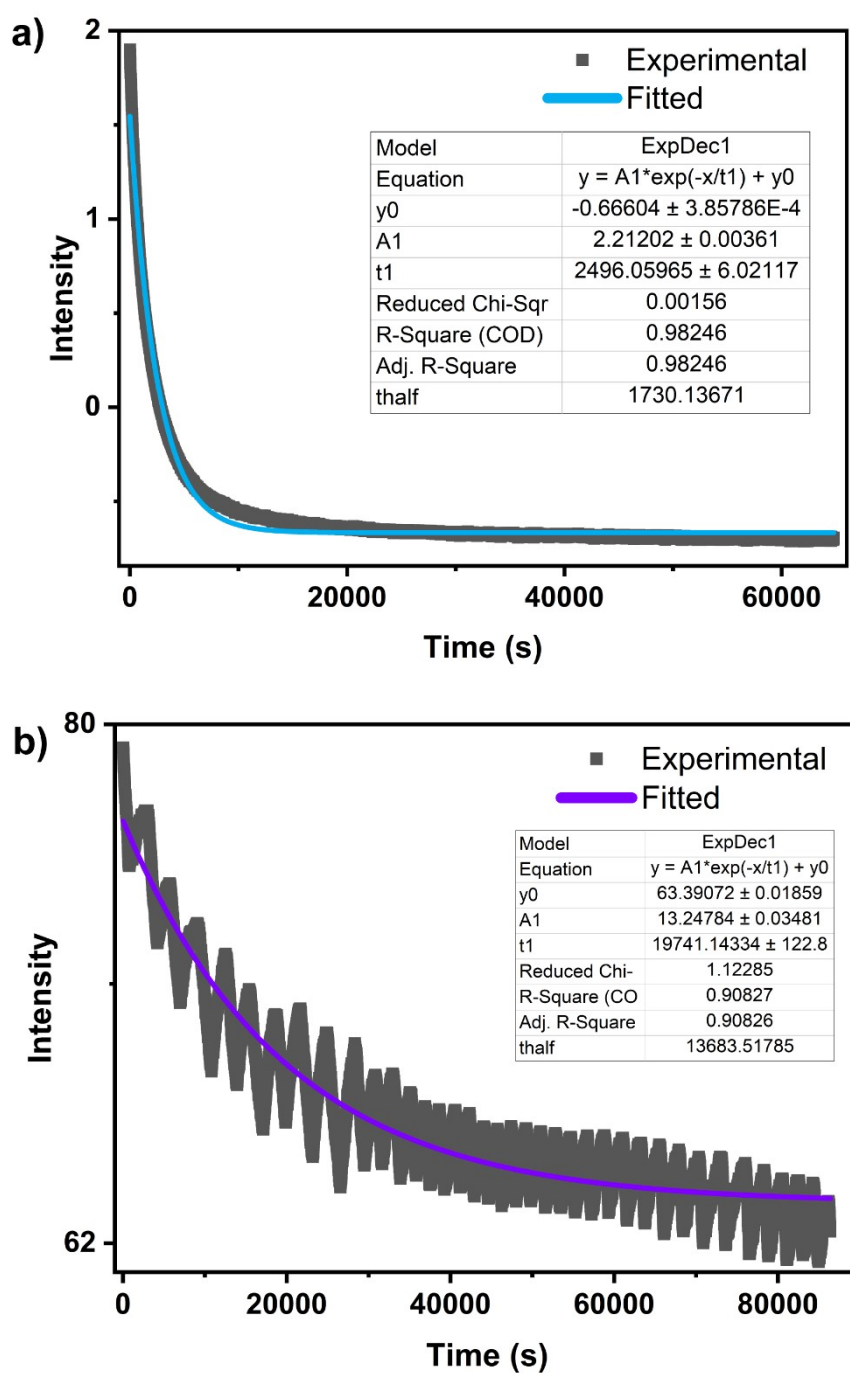


Figure S6: Time-delayed relaxation curves of EPR signal and fitted kinetic decay curves of a) **Zn-MOF** and b) **Cd-MOF**.

UV-Visible Spectra

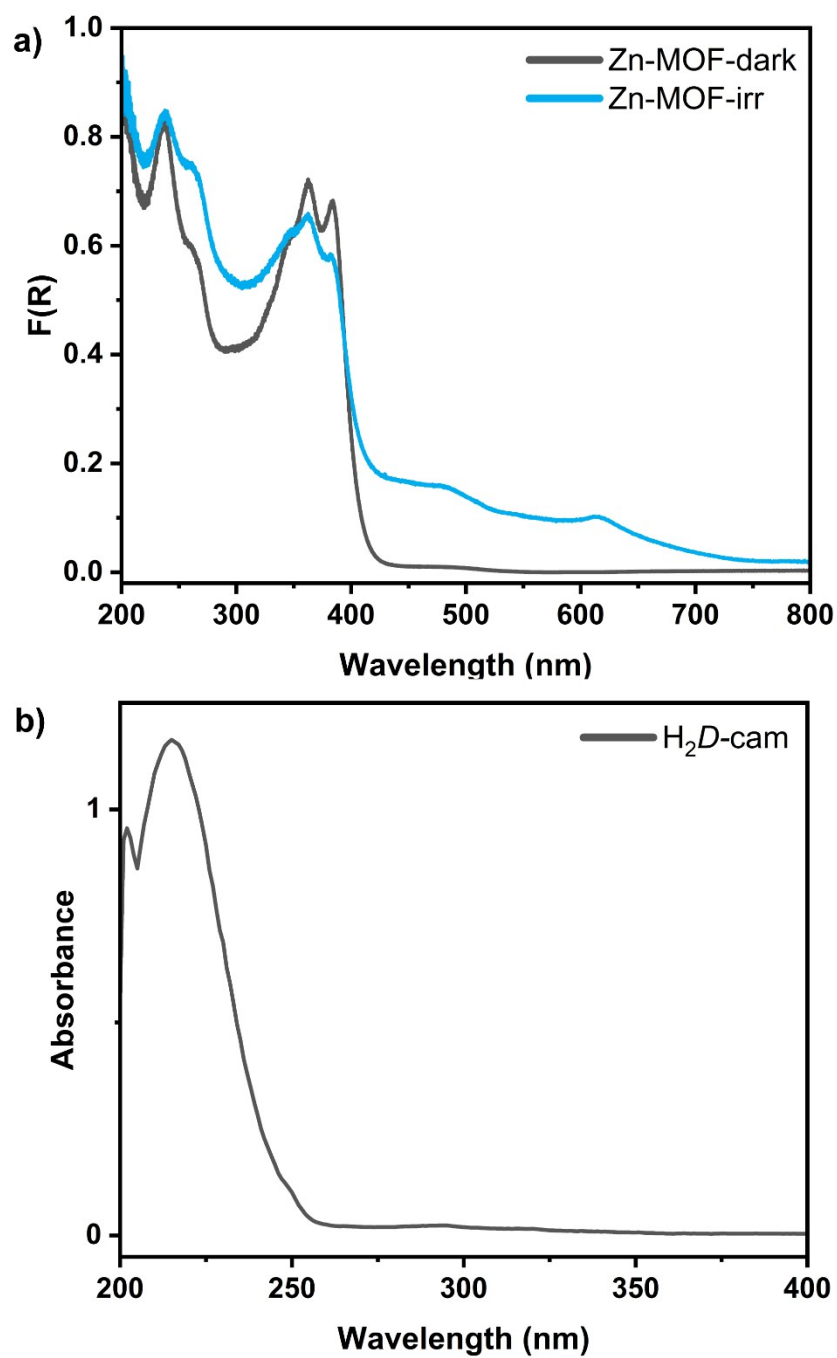


Figure S7: a) Diffuse reflectance spectrum of dark and irradiated states of **Zn-MOF** and; b) solution state absorbance spectrum of **H₂D-cam** in acetonitrile.

Near-IR Spectra

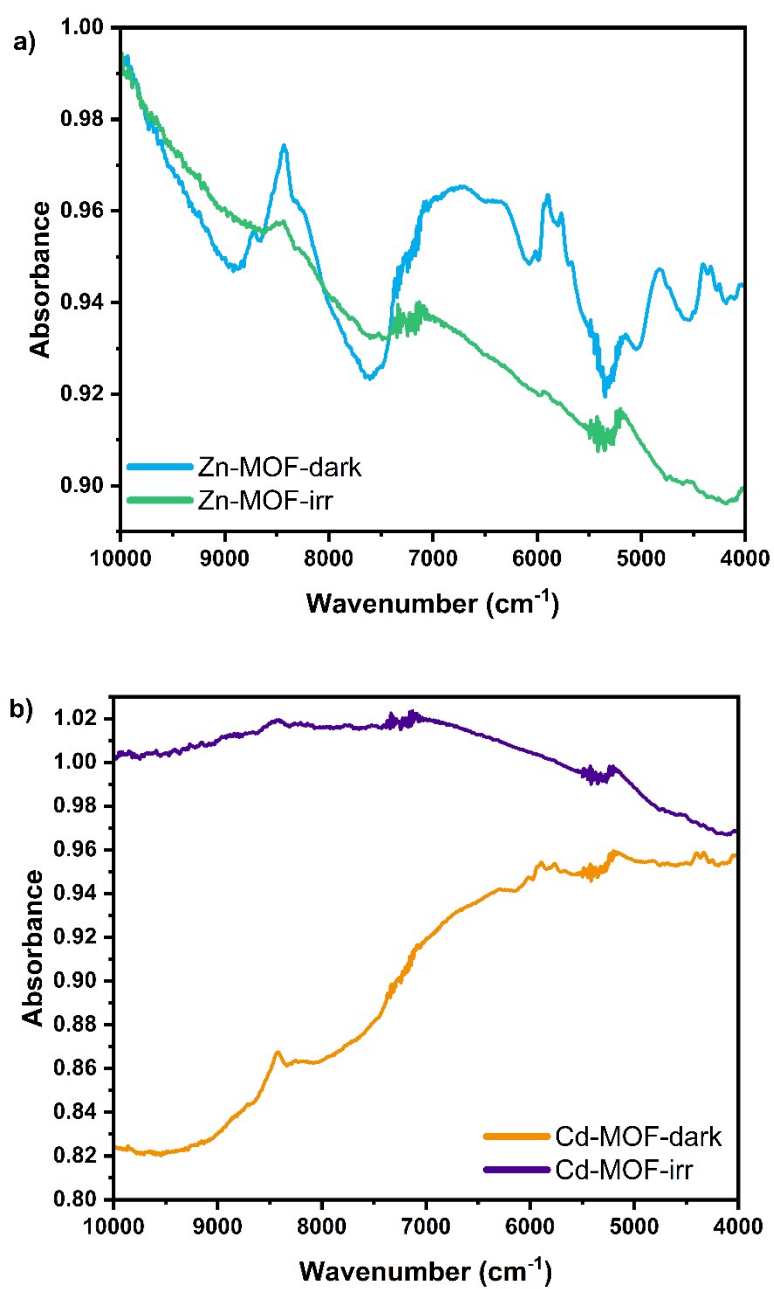
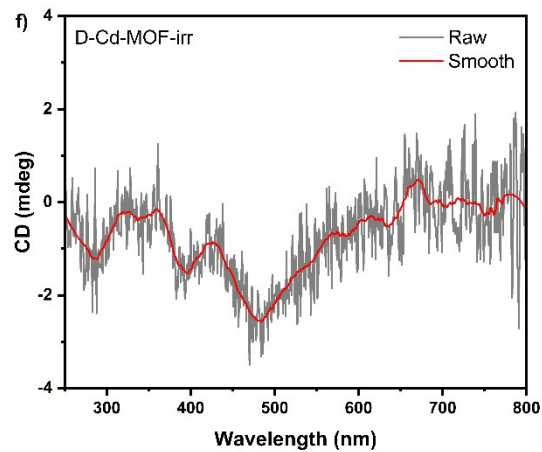
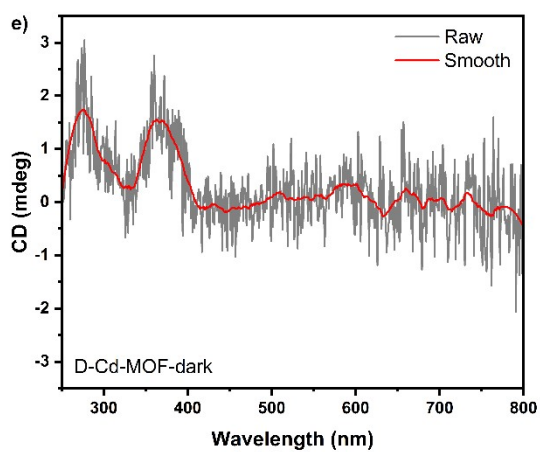
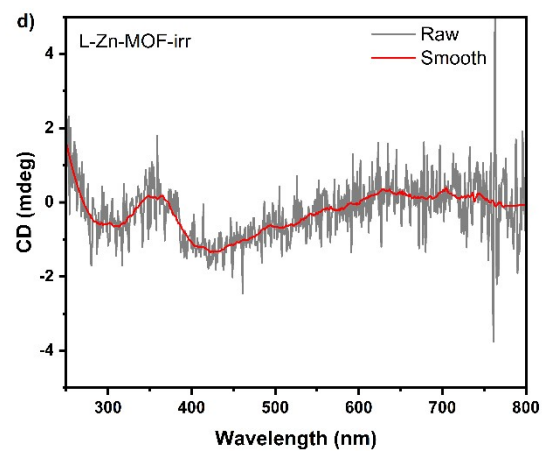
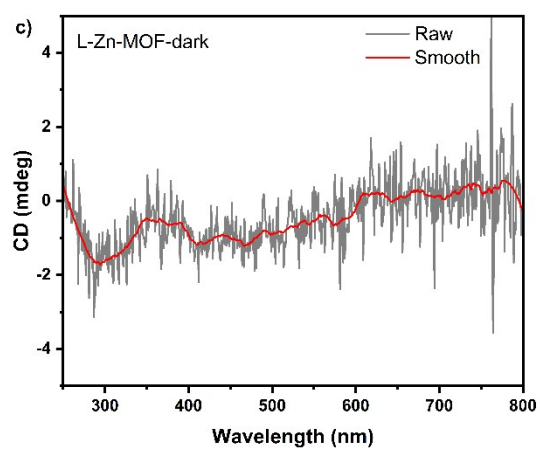
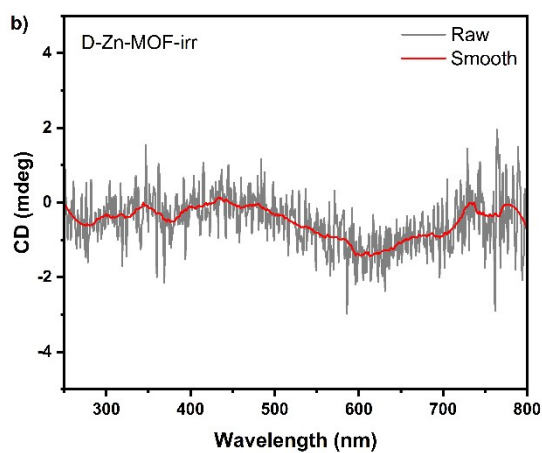
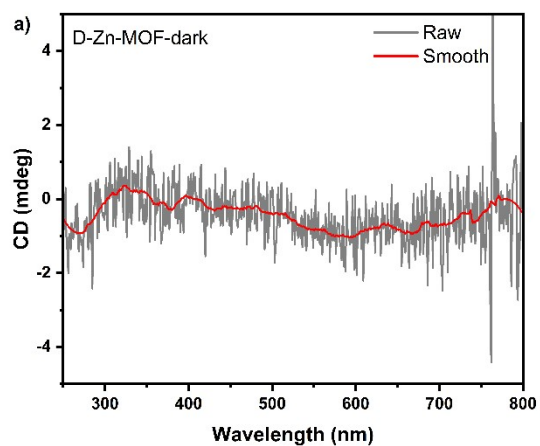


Figure S8: Near-IR spectrum of dark state (dark) and irradiated (irr) a) **Zn-MOF** and b) **Cd-MOF**. The absorbance bands observed between 8200-8700 cm^{-1} are attributed to background EtOH.

Circular Dichroism (CD) Spectra



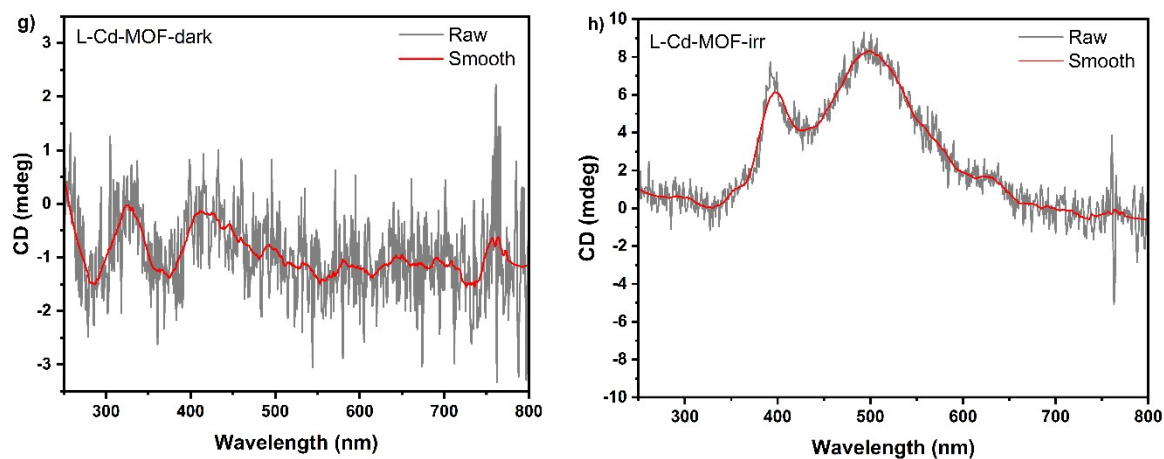


Figure S9: Raw and smoothed circular dichroism spectrum of a) **D-Zn-MOF-dark**, b) **D-Zn-MOF-irr**, c) **L-Zn-MOF-dark**, b) **L-Zn-MOF-irr**, e) **D-Cd-MOF-dark**, f) **D-Cd-MOF-irr**, g) **L-Cd-MOF-dark**, h) **L-Cd-MOF-irr**. Smoothing was calculated using Origin Pro 2022 software with Savitzky-Golay method with 50 points of window. Data points from 761-765 nm are instrument artefact.

Supporting Crystal Structure Images of D-Cd-MOF

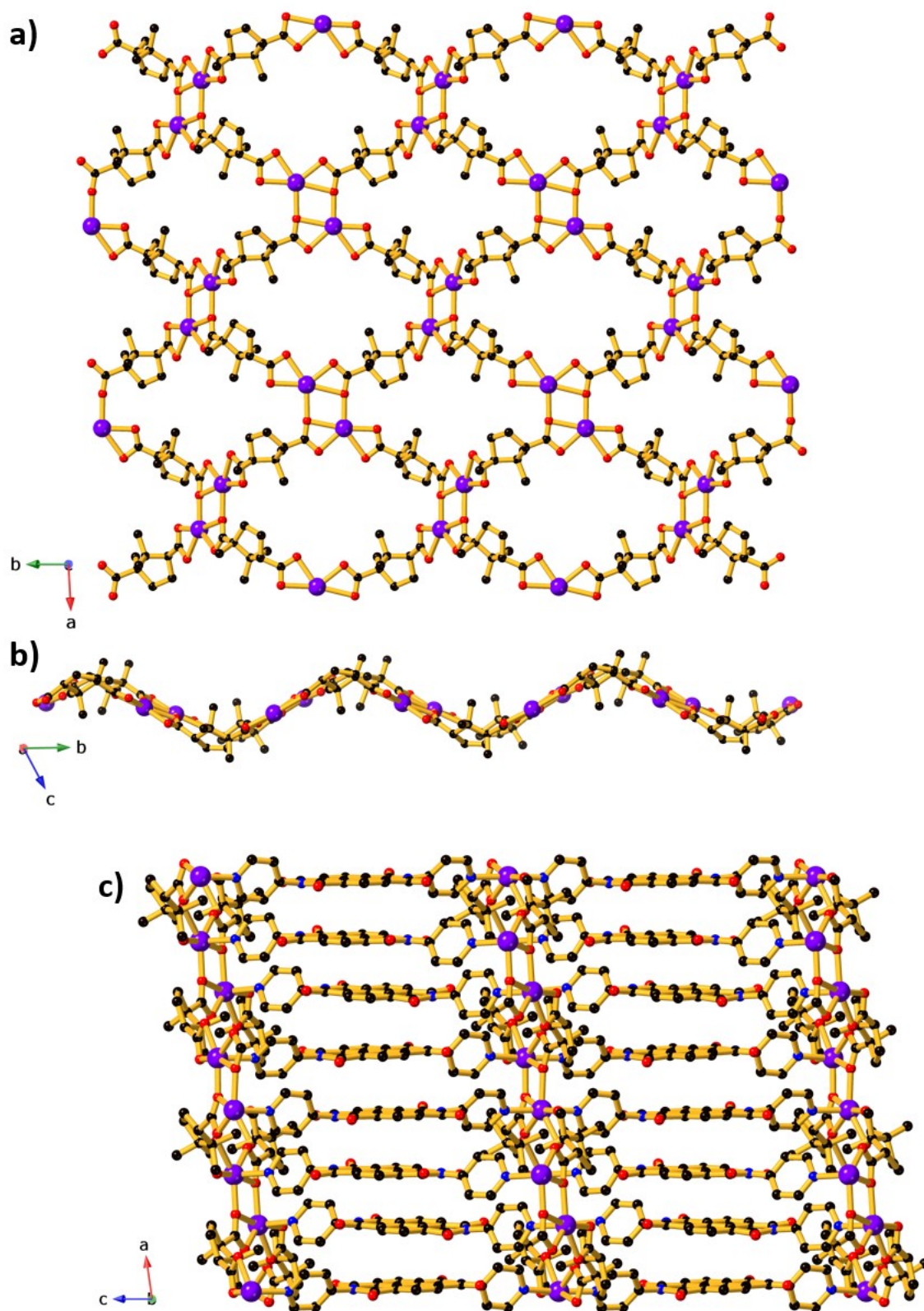


Figure S10: a) 2-D sheet of Cd-cam propagating down the a - b plane, b) view of the 2-D sheet down b -axis, highlighting waved or zig-zag shaped and, c) view of stacked DPNDI bridging the 2-D sheets down in D-Cd-MOF.

CD Reversibility Studies in Cd-MOF

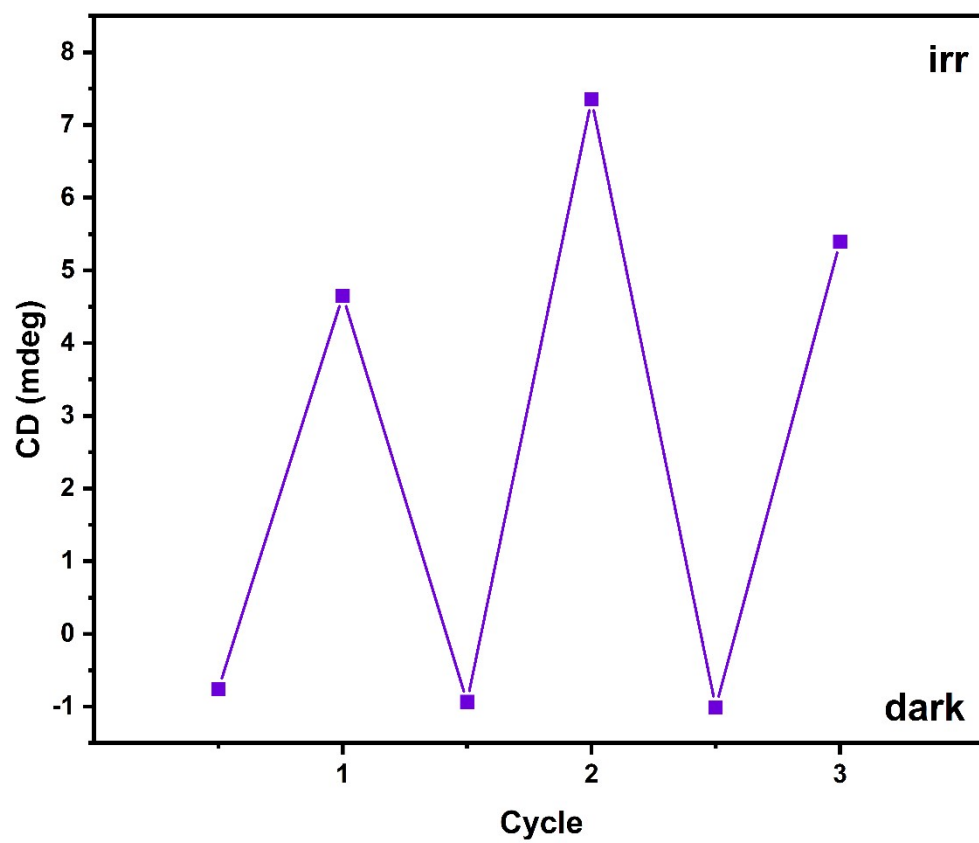


Figure S11: CD signal of L-Cd-MOF at 500 nm after three irradiation cycles.

References

1. G. M. Sheldrick, *Acta Crystallogr. Sect. A: Found Adv.*, **2015**, *71*, 3–8.
2. G. M. Sheldrick, *Acta Crystallogr. Sect. C Struct. Chem.*, **2015**, *71*, 3–8.
3. O. V. Dolomanov, L. J. Bourhis, R. J. Gildea, J. A. K. Howard, H. J. Puschmann, *Appl. Crystallogr.*, **2009**, *42*, 339–341.
4. T. J. Pilkington, M. W. Bignucolo, J. P. Ainsworth and S. Siemann, *Anal. Biochem.*, 2023, **678**, 115269.
5. P. H. Dinolfo, M. E. Williams, C. L. Stern and J. T. Hupp, *J. Am. Chem. Soc.*, 2004, **126**, 12989-13001.